doi:10.1016/j.jmb.2005.10.015 J. Mol. Biol. (2005) 354, 1081–1090

JMB

Available online at www.sciencedirect.com

SCIENCE DIRECT®

ELSEVIER

Structural Consequences of the pH-induced Conformational Switch in *A. polyphemus* Pheromone-binding Protein: Mechanisms of Ligand Release

Sergey Zubkov[1], Angela M. Gronenborn[3], In-Ja L. Byeon[3] and Smita Mohanty[1,2]*

[1]*Department of Biochemistry and Cell Biology, Stony Brook University, Stony Brook NY 11794-5215, USA*

[2]*Department of Chemistry and Biochemistry, Auburn University, Auburn AL 36849-5312, USA*

[3]*Laboratory of Chemical Physics National Institute of Diabetes and Digestive and Kidney Diseases, National Institutes of Health, Bethesda MD 20892 USA*

**Corresponding author*

Olfaction in moths is one of the most impressive examples of chemical communication found in nature for its exquisite sensitivity and selectivity. Pheromone-binding proteins (PBPs), present in the antennae of male moth and other insect species, bind the hydrophobic pheromone molecules and transport them to the G protein-coupled olfactory receptor proteins. The targeted delivery of these non-polar ligands to membrane-bound receptors involves ligand release on or near the target cell membranes, the molecular details of which are still not well understood. The PBP from the giant silk moth *Antheraea polyphemus* (ApolPBP) binds acetate pheromone only at pH above 6.0, and its structure at pH 6.3 has been determined previously. Here we report the solution NMR structure of ApolPBP at the acidic pH 5.2. Comparison of the present structure to that at neutral pH reveals the details of the pH-induced conformational changes and provides mechanistic clues for ligand release at acidic pH. The ApolPBP pH-induced structural change is quite different from that observed for alcohol binding *Bombyx mori* PBP (BmorPBP), where the C-terminal segment folds into a helix and occupies the ligand binding cavity. We observe a reorientation of helices α1, α3, and α4 at acidic pH caused by protonation of His69, His70 and His95 in the interior. This provides the driving force behind the opening of the ligand binding cavity and the release of the pheromone molecule from its carrier protein near the membrane.

Keywords: *Antheraea polyphemus*; pheromone-binding protein; olfaction; NMR structure; signal transduction

Introduction

Communication *via* chemical sensing is critical for all animals,[1,2] guiding their most fundamental behavior. Indeed, chemical sensing is essential for feeding, mating, avoiding toxic substances and withdrawing from hostile environments. The olfactory system enables animals to detect and discriminate between thousands of odorants in the environment. In fact, as much as 4% of the genome of many higher eukaryotes is devoted to encoding the proteins of "smell".[3] The olfactory repertoire is represented by a plethora of small organic molecules of varied carbon chains with diverse functional groups, including acetates, alcohols, aldehydes, etc. At the receiving end, olfactory receptors of both insects[4] and humans[5] are exquisitely capable of detecting and identifying single odorant molecules. One of the most extensively studied systems of chemical communication is the pheromone detection in moths.[6] It is characterized by extreme sensitivity, selectivity, and speed, allowing male moths to detect and follow turbulent wind-borne pheromone plumes left by the females.[7] Binding of a volatile hydrophobic odorant molecule by the odorant-binding protein (OBP) represents the very first step in the cascade of signal transduction events triggered by the activation of

Abbreviations used: PBP, pheromone-binding protein; GPCR, G protein-coupled receptor; OBP, odorant binding protein; GOBP, general OBP; ApolPBP, *Antheraea polyphemus* PBP; HSQC, heteronuclear single quantum correlation; NOE, nuclear Overhauser effect; NOESY, NOE spectroscopy; rms, root mean square; rmsd, rms deviation.

E-mail address of the corresponding author: smita.mohanty@stonybrook.edu; mohansm@auburn.edu

the G-protein-coupled receptor (GPCR).[8] OBPs are highly soluble acidic proteins with a molecular mass of 14–16 kDa. These proteins are present at very high concentration (10 mM) in the sensillum lymph, the aqueous media surrounding olfactory neurons in the sensory hairs of moth antennae.[9,10] OBPs are classified into two subfamilies: pheromone-binding proteins (PBPs), found in male species only, and general odorant-binding proteins (GOBPs), found in both sexes.[11] The PBPs from different moth species share over 50% sequence identity and about 30% identity with GOBPs. The OBPs identified in other insects may share as little as 9% sequence identity with moth PBPs, but they all have highly helical structure and contain six strictly conserved cysteine residues.[12] The first PBP identified by its ability to bind acetate pheromones was the PBP from the giant silk moth *Antheraea polyphemus* (ApolPBP).[9] At present, three PBPs have been identified in this species: ApolPBP, ApolPBP2, and ApolPBP3, each binding one component of the acetate pheromonal blend.[13] Although all PBPs show specificity in binding their respective pheromones,[13–15] they are also able to bind other ligands,[16,17] albeit with lower affinity. It has been suggested that each PBP binds to a range of similar molecules, but the interactions with the pheromone are unique and specific.[18,19] Furthermore, recent studies show that PBPs not only transport pheromones to the receptors, but also play an active role in receptor activation. Indeed, olfactory receptor activation requires PBP–pheromone complexes, rather than the pheromones alone.[20,21]

X-ray structures of PBPs from four insects have been determined: moth *Bombyx mori*,[22] cockroach *Leucophea maderae*,[23] honeybee *Apis mellifera*[24] and fruit fly *Drosophila melanogaster*.[25] Solution NMR structures have been characterized for two moth species: *B. mori*[26,27] and *A. polyphemus*.[28] These structural studies clearly show that all insect PBPs belong to a class of helical proteins that exhibit similar overall architecture and contain a deeply buried cavity within their interior. Despite this similarity, a large number of differences in the relative positioning of the helices and loops is observed, as well as variability with respect to amino acid type for the residues that line the binding cavity. The odorant molecule is accommodated in the hydrophobic cavity, but the exact mechanisms of pheromone entry and release remain to be clarified. A conformational change induced by pH has been reported for *B. mori*[26,29] and *A. polyphemus*[28,30] PBPs and is thought to be important for ligand release. It has been shown that conformational change in *B. mori* PBP is induced by both pH and by interaction with model membranes,[29] suggesting a possible mechanism for ligand release upon interaction of PBP–pheromone complex with the olfactory neuron. The pH near the membrane is more acidic than the bulk solution pH (sensillum lymph) due to the fact that the membrane potential decreases the local pH near the membrane.[31] For *B. mori* PBP, it was observed that the C-terminal portion (residues 125–137), which is essentially unstructured at neutral pH, undergoes a conformational change to a well-formed α-helix at acidic pH and inserts into the ligand-binding cavity, possibly displacing the pheromone molecule.[26,27] Although appealing, this ligand release mechanism[26] is unlikely to occur in other insect PBPs with known structures: in the honeybee[24] and fruit fly[25] PBPs the C-terminal residues are a part of the binding pockets in the ligand-bound conformation, while in the cockroach[23] PBP the C-terminal tail is missing entirely.

All PBPs with known structures belong to different insect orders: Lepidoptera (*B. mori*), Dyctioptera (*L. maderae*), Hymenoptera (*A. mellifera*), and Diptera (*D. melanogaster*), and although *B. mori* and *A. polyphemus* both belong to the Lepidoptera order, it is impossible to ascertain whether the mechanism proposed for *B. mori* PBP[26] applies generally for the entire order or whether it is strictly species-specific.[19,21] In fact, PBP from the gypsy moth *Lymantria dispar*, also belonging to the Lepidoptera order, binds its pheromone even at acidic pH,[32] suggesting that its ligand release mechanism may well be different from that of the *B. mori* PBP. Indeed, differences in ligand binding and release mechanism may be intimately connected to the chemical nature of the pheromone, an epoxide for *L. dispar* and an alcohol in the case of *B. mori*. In this context it should be pointed out that binding of a 14-carbon chain acetate pheromone by ApolPBP3 has been shown to occur at any pH.[13] Evaluating all currently available data together, it appears that the details of the pheromone binding and release for PBPs of each species are predominantly defined by the chemical structure of the pheromone, even if some general features may apply to all related PBPs.

In order to investigate the nature of the pheromone binding and release mechanisms, we initiated a comprehensive structural study of ApolPBP by NMR. This PBP has specific acetate-binding function *in vivo*. A conformational change in the protein was observed between pH 5 and 6,[28,30] suggesting a structural explanation for the loss of pheromone binding observed for this protein upon acidification.[33] Our solution NMR structure of ApolPBP at neutral pH[28] revealed the details of the acetate-binding site and provided the first insight into the nature of the pheromone uptake mechanism. Here we report the solution NMR structure of ApolPBP at acidic pH and propose a novel mechanism of pH-mediated pheromone release in *A. polyphemus*.

Results

Resonance assignments and analysis

The 2D {^{1}H,^{15}N} heteronuclear single quantum correlation (HSQC) spectrum of ApolPBP at 35 °C at pH 5.2 is shown in Figure 1. This spectrum is quite

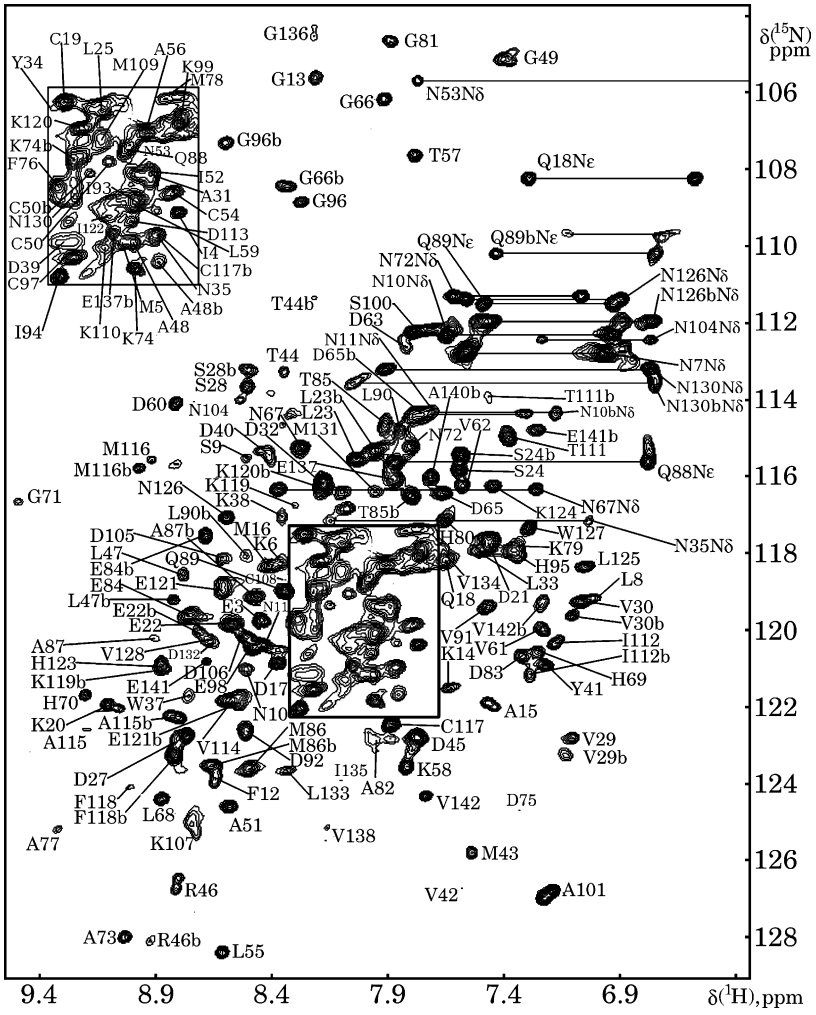

Figure 1. 2D {^{1}H,^{15}N} HSQC spectrum of the acidic form of ApolPBP at 35 °C. Assignments are indicated using the single letter amino acid code and the residue number. Side-chain NH_2 resonances of asparagine and glutamine residues are connected by horizontal lines. Side-chain resonances of N53 and the tryptophan residues and backbone resonances of N7, L139, and A140 reside outside the displayed region. Peaks labeled b correspond to the neutral pH form.

different from the one at pH values above 6. A secondary set of resonances (labeled b in the Figure) corresponds to resonances observed at higher pH, representing the neutral pH conformation of the protein (Figure 2). Residues with well separated, doubled resonances comprise ca 14% of the protein's primary sequence. Thus discrete conformational states are present for short polypeptide segments in the otherwise well folded protein, most likely associated with different protonation states of titratable residues such as Asp and Glu, whose pK_a values are around 4. Local conformational heterogeneity, in addition to the poor resonance dispersion typical for proteins with high helical content, complicates resonance assignments and renders structure analysis of the acidic form of ApolPBP a difficult task. Sequence-specific assignments were accomplished primarily using three-dimensional HNCACB, CBCACONH, and C(CCO)NH[34] experiments. 3D HNCO, HCACO, HSQC-TOCSY, and HC(CCO)NH[34] data were employed to resolve ambiguities arising from degeneracies in the ^{13}C frequency. Assignments of the N-terminal residues 1–10 and the segment 33–39 corresponding to a flexible loop in the pH 6.3 structure, were extremely challenging due to low resonance intensity and could only be completed with the help of 3D {^{13}C,^{1}H} HSQC-NOESY combined with HCACO experiments. The NMR assignment of ^{1}H, ^{13}C, and ^{15}N backbone resonances of ApolPBP at pH 5.2 is complete for all residues except Ser1 and Phe36. The assignment of the non-labile side-chain proton resonances is 92% complete. At this point we would like to emphasize that lowering the pH did not yield any improvements in the spectra. On the contrary, extreme broadening of resonances and changes indicative of acid-induced unfolding of the protein were observed. Therefore, the assignments and structure determination had to be carried out on a sample containing multiple species, a difficult and arduous task.

Analysis of the chemical shift difference between the neutral and acidic pH forms of ApolPBP (Figure 3(a)) revealed that the largest changes in amide resonance frequencies (greater than 1 ppm $\Delta\delta_{comp}$) occur for His95 and the residues in the polypeptide segment 54–72. This segment corresponds to helices α3b, α4, and the interconnecting flexible loop in the neutral pH structure.[28] The substantial chemical shift changes observed for residues His69, His70, and His95 suggest that they are related to changes in protonation states between

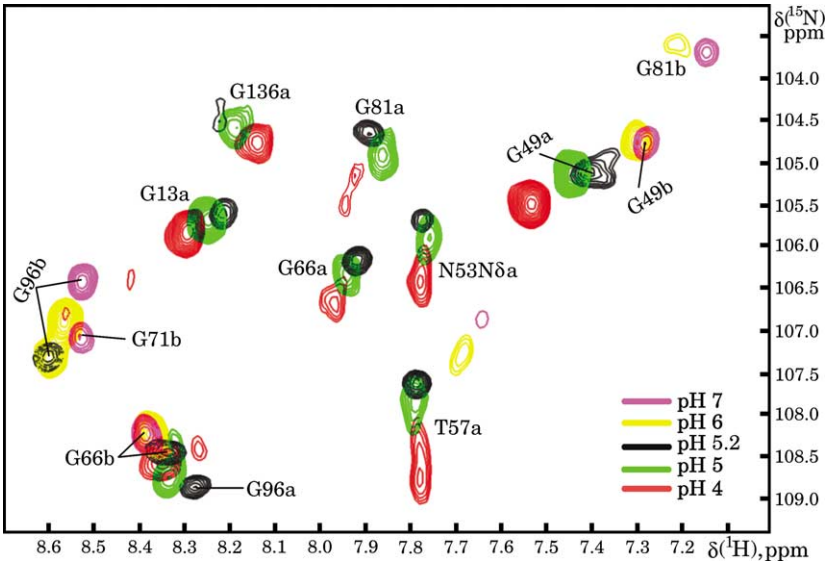

Figure 2. Expanded sub-region of the 2D {^{1}H,^{15}N} HSQC spectra of ApolPBP at different pH values, demonstrating the doubling of resonances at low pH. Assignments are indicated with single letter amino acid code, residue number, and suffix a or b, corresponding to the acidic or neutral pH[28] forms, respectively. Both a and b forms are present at pH 5.2.

pH 6 and 5, consistent with the NMR titration data obtained for the histidine side-chains that revealed pK_a values between 6.1 and 6.3 for all but two histidine residues, values that are commonly observed for histidine. Two histidine residues exhibit pK_a values of 5.1 and 5.3, close to the pH where the proposed conformational switch occurs. Resonance frequency changes for other residues in the flexible loop containing His69 and His70 are most likely caused by a conformational rearrangement brought about by interactions involving protonated His residues. Significant chemical shift differences between pH 6 and 5 were also observed for residues 3–18 and 31–39, which correspond to the N-terminal helices α1a and α1b and the flexible loop between α2 and α3a. Chemical shifts of residues in other secondary structure elements were not affected in a major way by the pH change, implying that only α3b, α4, α1a, α1b, and the associated flexible segments are altered significantly in the pH-induced conformational transition (Figure 5). An interesting pattern of chemical shift changes can be seen around the end of the helix α6, where several amino acids with significant chemical shift differences are evenly separated by those with small changes. This may be an indicator of a structural change that occurs in proximity of this protein segment so that the residues facing the altered area and those facing away exhibit different chemical shift sensitivity.

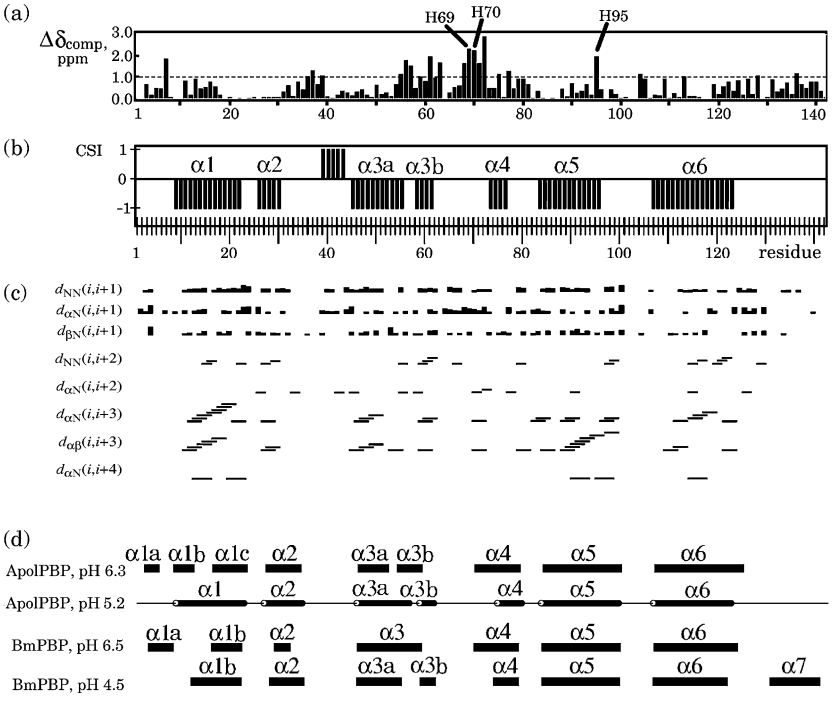

Figure 3. Secondary structure of ApolPBP at acidic pH. (a) Compound chemical shift difference between neutral and acidic forms. (b) Consensus (H$^\alpha$, C$^\alpha$, and CO) chemical shift index[34] of ApolPBP at acidic pH values of +1, 0 and −1 indicate b-sheet, random coil, and α-helical structure, respectively. (c) Summary of sequential NOEs. (d) Secondary structure of both neutral and acidic forms of ApolPBP as observed in the final ensemble of 20 energy-minimized conformations and for comparison that of BmPBP are shown here.

Secondary structure

Analysis of the chemical shift deviations for H^{α}, C^{α}, and CO from their random coil values,[35] as well as the backbone geometry obtained using the program TALOS,[36] revealed seven helical regions comprising residues 9–22, 27–33, 46–56, 59–62, 75–80, 84–100, and 107–125 (Figure 3(b)). These helices correspond, respectively, to α1c, α2, α3a, α3b, α4, α5, and α6 of the pH 6.3 form of ApolPBP.[28] Notable differences from the pH 6.3 structure, as indicated by the shift analysis, include changes in the exact positioning of α3b, a shortened α4 and the absence of the N-terminal segments of α1: at neutral pH helix α1 consists of three segments: α1a, α1b, and α1c, while only α1c exists at acidic pH (Figure 4).

Three-dimensional structure

The 142 residue ApolPBP structure at acidic pH consists of seven α-helices (Figures 4 and 5): α1 (9–23), α2 (27–35), α3a (46–57), α3b (59–62), α4 (75–80), α5 (84–100), and α6 (107–123), interconnected by three disulfide bridges. The helices are packed in an approximately globular structure (residues 9–123) with unstructured N and C termini. The two longest helices, α5 and α6, cross at an angle of 42°, with residues Ile93, Ile94, Leu90 and Phe118 forming the major hydrophobic contacts between them. They are also connected by the disulfide bridge between Cys97 and Cys117. Helix α3a is connected to α6 *via* Cys50–Cys108 and with a crossing angle of 76°. Here, residues Ile122 and Gly49 form the contact interface. Helices α1 and α2 form an αα-corner,[37] linked to α3a by the Cys19–Cys54 bridge. Helix α1 is packed against α3a with a 50° angle, typical for ridges-into-grooves helix packing. Residues Ala15, Leu55, Leu23, and Ala51 are involved in the hydrophobic interaction between these two helices and Val29, Val30, and Ala48 form the interface between α2 and α3a.

The N-terminal segment (residues 1–8) is largely unstructured and is positioned near helix α2, with the hydrophobic residue Ile4 shielded from the solvent. Residues in the short loop between α1 and α2 adopt backbone torsion angles characteristic of a three-residue αα-corner[37]: ϕ,ψ(S24) = +50°, +20°, ϕ,ψ(L25) = −83°, +166°, ϕ,ψ(P26) = −75°, +120°, although the crossing angle between these helices is 51°, deviating from the ideal angle of 90°. Similar to findings in the neutral pH structure, the flexible loop comprising residues 36–45 between helices α2 and α3a does not have a well defined structure and exhibits noticeable flexibility, except at its C-terminal portion, where Tyr41 and Val42 are involved in hydrophobic contacts with helix α6. The structure of the long polypeptide segment 58–75 between α3a and α4, however, is remarkably different from that at neutral pH and is well defined, as evidenced by a dense network of nuclear Overhauser effects (NOEs). It includes a 90° kink at residue Lys58, which positions the short helix α3b in such a way that the hydrophilic Asp60

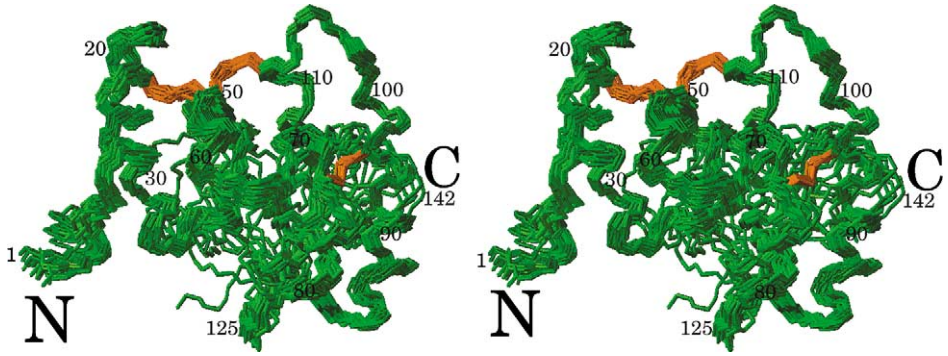

Figure 4. Stereo view of the ensemble of the 20 lowest energy structures of ApolPBP at acidic pH. The backbone is shown in green and the disulfide bonds in orange.

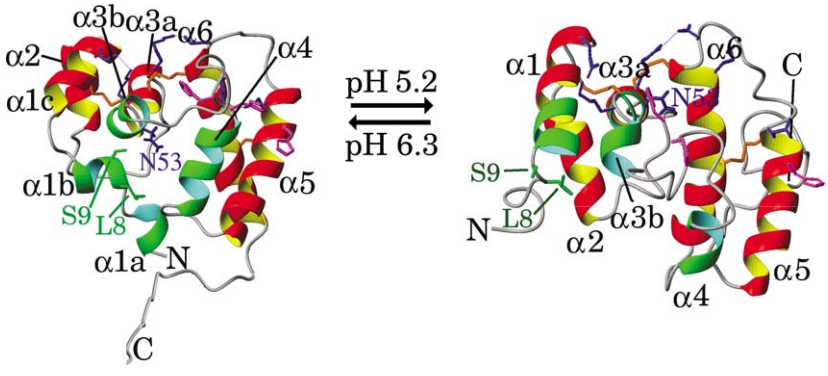

Figure 5. Ribbon view of ApolPBP neutral form (left) and acidic form (right). The side-chain of Asn53 and side-chains of the residues involved in salt-bridges are shown in blue. The side-chains of Leu8 and Ser9 are shown in green and the histidine side-chains of H69, H70, and H95 are shown in purple. The disulfide bonds are indicated in orange. The residues exhibiting large chemical shift changes are highlighted in green.

is solvent-exposed while Leu59, Val61, and Val62 face the hydrophobic core of the protein. A type I β-turn[38] is formed by residues Asp63-Leu66 (ϕ,ψ(P64) = −75°, −42°, ϕ,ψ(D65) = −111°, 2°) and a type II β-turn is formed by His69-Asn72 (ϕ,ψ(H70) = −42°, 140°, ϕ,ψ(G71) = 80°, −45°). A two-residue linker connects the second β-turn to helix α4. The C-terminal residues (124–142) and the short loops connecting helices α4, α5, and α6 exhibit no regular structure.

pH-induced changes

We observe a number of differences between the structures of ApolPBP at the neutral and acidic pH (Figure 5). For the helical regions, the root-mean-square deviation (rmsd) between the two structures is 4.7 Å. The most prominent structural change, already indicated by the chemical shift differences, is the restructuring of helix α3 and of the loop between α3 and α4. In the neutral pH structure we observe a kink in the middle of α3 that causes the side-chain of Asn53 to be a part of the pheromone binding pocket.[28] At acidic pH values, the kink disappears and the helix straightens at this point with Asn53 moving 8 Å away from the protein core, pointing towards the solvent. In the low pH structure, a distortion of helix α3 is now observed at Lys58 resulting in a shorter and differently positioned helix α3b. The entire loop between α3b and α4 is restructured, creating a substantial increase in the distances between the side-chains of His69, His70, and His95. The distance between the side-chains of His70 and His95 is 8.1 Å at neutral pH and 22.9 Å at acidic pH, measured between the closest ring protons. Another major change is the disordering of the short helices α1a and α1b at acidic pH, while helix α1c increases in length by five residues. This winding and unwinding of the N-terminal helices is in agreement with recent hypothesis from CD studies of ApolPBP.[54] Furthermore, as a consequence of the decrease in pH, all three salt-bridges, well defined in the neutral pH structure,[28] are disrupted. The distance between the side-chains of Arg46 and Asp106 is increased by 2 Å, between Lys110 and Glu98 by 6 Å, and between Lys58 and Glu22 by 10 Å or more.

Two conformations in the low pH structure

At the acidic pH we observed increased flexibility for two polypeptide segments of ApolPBP as indicated by very broad or missing NOE peaks, characteristic of local conformational exchange processes on an intermediate timescale. These are the N-terminal residues 1–10 and the segment 33–39, which is a part of a flexible loop between α2 and α3a. These two peptide segments are also flexible in the neutral pH structure.[28]

Doubling of resonances was noted for a number of residues, clearly reflecting two conformations for ApolPBP under the current experimental conditions. At acidic pH, residues that exhibit two resonances are mainly localized in the segments 22–32, 64–100, and 136–142, comprising α2, the large α3b–α5 segment, and the very end of the disordered C-terminal segment. One set of the resonances is similar in chemical shift values to those of ApolPBP at neutral pH (Figure 2) and the intensities of the affected residues suggest a ratio of the neutral pH state as high as 30–40%. The most likely explanation for the distinct second set of resonances is a conformational transition involving the long loop α3b–α4, which may have little structural consequences for the overall architecture of the protein. Considering the complexity of the conformational switch between the neutral and the acidic pH forms of ApolPBP, it is not surprising that this segment is flexible at both acidic and neutral pH.[28]

Discussion

Based on the three-dimensional structures of ApolPBP at neutral[28] and acidic pH, we propose the following mechanism for the pheromone release (Figure 6). Upon acidification, protonation of the imidazole rings of His69, His70, and His95 occurs in a concerted manner (Figure 6(a)); the three positively charged side-chains come into close contact and therefore mutual repulsion occurs. pH-triggered conformational switch involving histidine(s) protonation/deprotonation is a regulatory mechanism for many proteins such as retinol-binding protein,[39] serum transferrins,[40] prion protein[41] and human NADPH oxidase.[42] The unfavorable interaction between the positively charged histidine residues in ApolPBP leads to a dramatic change in the position of His95, rotating helix α5 by 60° counter-clockwise around its axis (Figure 6(b), step 1). This rotation pulls on the Cys97-Cys117 link, and the protonation of Asp106 disrupts the salt-bridge between Arg46 and Asp106, resulting in a change of position of helix α6. This helix moves inward towards the protein core, resulting in the reduction of its crossing angle with α5 by 20° (Figure 6(b), steps 2 and 3). This effect is in turn transmitted to helix α3 *via* the Cys50–Cys108 link and contributes to the straightening of this helix (Figure 6(b), step 4). At the same time, residues His69 and His70 move away from His95 and from one another due to charge repulsion (Figure 6(c), step 1), taking the α3b–α4 loop with them and thereby forcing it to adopt a remarkably different conformation from that observed at neutral pH. The C-terminal end of α3b, no longer connected to α2 by the Lys58–Glu22 salt-bridge, moves towards the protein's N terminus (Figure 6(c), step 2) also contributing to the straightening of helix α3 (Figure 6(c), step 3). Once helix α3 loses the kink at Asn53, the interaction between α1b and α3 is also disrupted and helix α1 straightens out, although it becomes unstructured at the N terminus (Figure 5). Concomitant loss of the kink with the straightening of α3 moves the Asn53 side-chain 8 Å away from its original position inside the pheromone binding cavity, disrupting the interaction with the ligand.

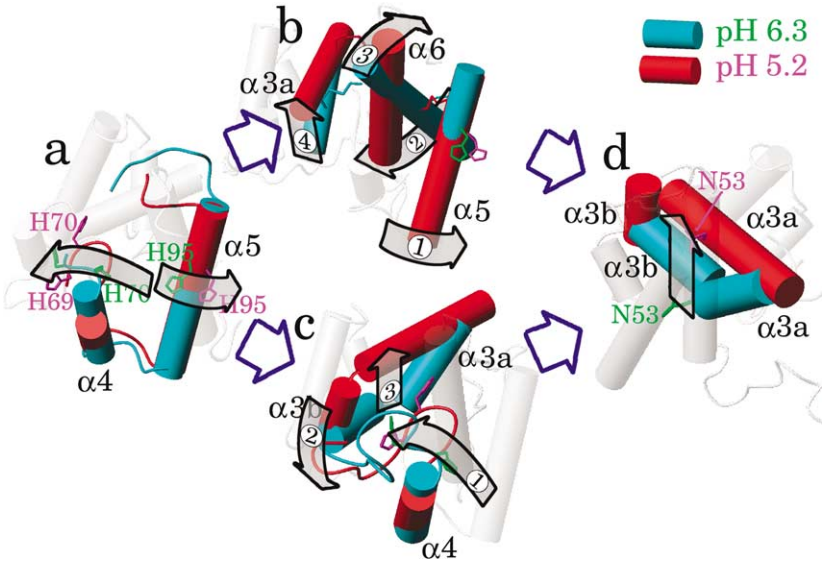

Figure 6. Proposed mechanism of the pH-induced conformational transition. Helical fragments are shown as cylinders, labeled, and colored red in the acidic pH and cyan in the neutral pH structures. Grey colored arrows indicate the structural changes that occur at pH change from 6.3 to 5.2. Light grey cylinders show the rest of the pH 5.2 structure for context. (a) Repulsion between the protonated histidine residues. (b) Propagation of the movement of His95 through the 3D structure. (c) Propagation of the movement of His70 through the 3D structure. (d) Final restructuring of the helix α3.

The change in the structure of helix α1 opens the cavity entrance, allowing the ligand to be released.

The potential importance of the histidine residues for PBP function was first suggested by Sandler *et al.* for *B. mori* PBP, based on histidine positions in the crystal structure.[22] It has also been shown by circular dichroism spectroscopy that His69 and His70 in ApolPBP are directly involved in pheromone binding.[19] Remarkably, His69, His70, and His95 are strictly conserved through lepidopteran PBPs and GOBPs,[43] suggesting that their role in the OBP function may be general for the entire order.

Earlier we suggested that the side-chains of the residues 8 and 9 may serve as the determinants of the bound pheromone chain length,[28] since the smaller amino acids, Leu8 and Ser9, are found in the PBPs of the species that use 16-carbon pheromones while the larger residues, Met8 and Thr9 are found in the species that use 14-carbon pheromones. A recent study by Maida *et al.*[13] revealed that ApolPBP and ApolPBP3 from *A. polyphemus* preferably bind 16-carbon and 14-carbon acetate pheromones, respectively, although they share 52% sequence identity. The primary sequence of ApolPBP contains Leu8 and Ser9, while in ApolPBP3 Met8 and Thr9 are found. These new data provide additional support for our proposed pheromone selection mechanism.[28] In ApolPBP, these two residues are part of the polypeptide segment in helix α1b at neutral pH, positioning Leu8 and Ser9 in the binding cavity, whereas at acidic pH, this polypeptide chain is unstructured, allowing the cavity to open (Figure 5). If the side-chains of Leu8 and Ser9 are indeed interacting with the hydrocarbon chain of the bound pheromone, this offers an elegant mechanism for ligand release. The N-terminal part of the helix α1 acts as a removable lid, enclosing the ligand at pH 6 but allowing its release at low pH.

Our structure of ApolPBP at acidic pH presents us with the first possibility to compare the non-binding conformations of two lepidopteran PBPs that share 67% sequence identity: ApolPBP and *B. mori* PBP.[26] Two important features of the conformational transition appear to be common for both moth species: unfolding of the N-terminal helices (α1a for *B. mori* PBP, α1a and α1b for ApolPBP) and a well-defined conformation at acidic pH for the polypeptide segment 58–72, including the kink at Lys58, the short helix α3b, and the two subsequent β-turns. However, a major difference exists for these two proteins: in ApolPBP we note the complete absence of the C-terminal helix α7. This is immediately apparent from an inspection of chemical shift values, which are non-helical, and from the lack of any sequential NOEs in this polypeptide segment (Figure 3(c)). Apparently, internalization of the C terminus in form of a helix into the binding cavity at acidic pH is not a general feature of all lepidopteran PBPs. This structural difference is likely caused by the difference in the position of the crucial polar residue (Asn53 in ApolPBP and Ser56 in *B. mori*. PBP). In the case of *B. mori*, helix α3 is straight and the residue responsible for pheromone headgroup interaction (Ser56) is found inside the cavity at both neutral[27] and acidic pH.[26] It is possible that at low pH the cavity in *B. mori* PBP opens due to unfolding of α1a, similar to ApolPBP, but since Ser56 does not move away, helix α7 can form and competitively displace the ligand from the open binding cavity. Therefore, pheromone binding and release mechanisms are clearly different in these related PBPs as a result of a notable difference in the structure of the pheromone binding site, consistent with the different chemical structure of the respective ligands.

Conclusion

We present a novel mechanism of pheromone release by the PBPs, triggered by protonation of

the key histidine residues near the olfactory neuron where the membrane potential decreases the local pH as compared to the pH of the bulk of the solution[31] (at sensillum lymph). Our model takes into account the following experimental evidence: changes of chemical shifts and NOE resonances caused by the change in the pH, resulting in a major conformational switch in the three-dimensional structure, pK_a values and the strict conservation of the histidine residues throughout lepidopteran OBPs. This pH-triggered conformational change in ApolPBP results in deactivation of the ligand headgroup binding site and opening of the binding cavity, facilitating ligand exit between the C-terminal end of α6, the N-terminal end of α1, and the loop connecting α2 and α3a. The details of the conformational switch differ between PBPs from different moth species and appear to depend on the structure of the binding site, in particular the amino acid residues lining the binding cavity, and on the chemical structure of the pheromone.

This above mechanism represents an important new step towards understanding the molecular details of chemical messenger perception and recognition. The structural and biological data accumulated on insect OBPs will open up possibilities for detailed mechanistic proposals for perireceptor events in olfaction. Such basic understanding will in turn, have a far-reaching impact in such areas as agricultural pest control,[44] biological modeling of single-molecule chemosensors[45] and artificial odor-tracking systems.[46]

Materials and Methods

Protein expression and sample preparation

Recombinant ApolPBP, consisting of 142 residues, was expressed in *Escherichia coli*, purified and refolded as reported earlier.[28] The NMR sample contained ~1 mM uniformly $^{15}N/^{13}C$-labeled ApolPBP in 50 mM phosphate buffer (pH approx. 5.2 at 35 °C), 1 mM EDTA, 0.1% (w/v) NaN_3, 95% H_2O and 5% ^2H_2O.

NMR experiments

All NMR data were collected on Bruker DMX 600, DMX 750, and DRX 800 spectrometers at 35 °C. The following NMR experiments[34] were performed for the purpose of sequential assignment: 2D {^{15}N,^1H} HSQC (Figure 1), 3D HNCACB, 3D CBCACONH, 3D HCACO, 3D HNCO, 3D C(CCO)NH, 3D HC(CCO)NH, 3D HSQC-TOCSY, 3D {^{15}N,^1H} HSQC-NOESY, and two 3D {^{13}C,^1H} HSQC-NOESY experiments with the ^{13}C carrier frequency in the aliphatic (43 ppm) and aromatic (125 ppm) regions, respectively. The NOE spectra were collected with mixing times of 150 ms for {^{15}N,^1H} HSQC-NOESY and 120 ms for {^{13}C,^1H} HSQC-NOESY. The NMR data were processed using NMRPipe[47] and analyzed with NMRView.[48] The secondary structure information was derived from the assigned chemical shifts with the programs CSI[35] and TALOS.[36] To express changes in the chemical shifts of the individual residues, a compound chemical shift change (Δδ, ppm) was defined as $\Delta\delta_{comp} = [\Delta\delta_{HN}^2 + (\Delta\delta_N/R_{scale})^2]^{1/2}$, where the chemical shift scaling factor R_{scale} was set to 6.5.[49]

Structure calculation

A total of 2924 NOE cross-peaks were assigned manually using NMRView.[48] Of these, 419 peaks were identified as either ambiguously assigned or belonging to the residues labeled b in Figure 1 (local conformers similar to the neutral pH form) and removed from structure calculation. The experimental upper distance restraints were derived from the intensities of the assigned NOE signals with the program CYANA,[50] using two calibration functions: d^{-6} for the backbone and d^{-4} for the side-chain resonances. Because the conformational heterogeneity in ApolPBP at low pH is non-uniform, intensity of the cross-peaks involved in it could not be adjusted reliably and the distance restraints were relaxed, assuming the worst-case scenario in each case. After elimination of redundant and non-restraining restraints, the final set of 1469 experimental distance restraints was taken for structure calculation (Table 1). A total of 272 dihedral angle restraints were obtained with the program TALOS[36] based on the assigned chemical shifts. Of these, 68 best ranked restraints were used directly with the allowed range of torsion angles set to 5 deg. The other 204 restraints were compared to the results of preliminary structure calculations, adjusted to allow wider ranges of torsion angles (10–100 deg.), and used in the final structure calculation. Additionally, 110 hydrogen bond upper distance restraints (two restraints per bond) were derived from the CSI[35] output by ARIA.[51] The structure of ApolPBP was calculated by torsion angle dynamics simulated annealing as implemented in the program CYANA.[50] The length of the annealing procedure was increased to 16,000 steps and the starting temperature was set to 20 CYANA units. Calculations were performed for 500 randomized starting conformations and the 20 structures with the lowest target function values (Figure 4) were selected for further analysis.

Table 1. Structural statistics for ApolPBP at pH 5.2

Property	Value
Restraints	
Total experimental distance restraints	1469
Intraresidue ($\|i-j\|=0$)	753
Sequential ($\|i-j\|=1$)	401
Medium range ($2\leq\|i-j\|\leq4$)	230
Long range ($\|i-j\|\geq5$)	85
Hydrogen bond distance restraints	110
Dihedral angle restraints	272
Residual restraints violations in the ensemble of 20 structures	
Distance restraint violations greater than 0.2 Å	13±5
Maximal distance restraint violation (Å)	0.53±0.11
Dihedral angle restraint violations greater than 5°	3±2
Maximal dihedral angle violation (deg.)	6.56±1.50
rms deviations from the averaged coordinates (Å)	
Backbone of the regular secondary structure	0.52
All heavy atoms of the regular secondary structure	0.96
Backbone of the residues 10–125	0.56
All heavy atoms of the residues 10–125	1.08
Ramachandran plot statistics (%)	
Most favored regions	74.1
Additionally allowed regions	24.0
Generously allowed regions	2.0
Disallowed regions	0.0

Statistics and visualization

Visualization, rms deviation, and interatomic distance measurements were carried out with the program MOLMOL.[52] Ramachandran plot statistics were calculated with PROCHECK.[53]

Histidine pK_a calculation

Two-dimensional $\{^{15}N,^{1}H\}$ HMQC spectra were acquired for ApolPBP at 35 °C over a pH range of 4.7–8.7. ^{15}N offset frequency was set to 210 ppm, ^{1}H offset was 4.68 ppm. The delay during which ^{15}N and ^{1}H signals become antiphase was set to 22 ms to refocus magnetization arising from $^{1}J_{NH}$ couplings. Cross-peaks between the histidine side-chain atoms $N^{\delta1}$, $N^{\varepsilon2}$, $H^{\varepsilon1}$, $H^{\delta2}$ were observed for all histidine residues. The ^{1}H and ^{15}N chemical shifts of the histidine side-chains were plotted against pH values. The pK_a values were determined from the one-proton titration curve $\delta_{obs} = \delta_{HA} + (\delta_A - \delta_{HA}) \times 10^{-pK_a}/(10^{-pK_a} + 10^{-pH})$, where δ_{obs} is the observed chemical shift, δ_{HA} and δ_A are the chemical shifts for the protonated and non-protonated forms, respectively. The titration data were fitted by non-linear regression using the program gnuplot.

Protein Data Bank accession code

The atomic coordinates (code 1TWO) of the acidic pH structure of ApolPBP have been deposited in the Protein Data Bank, Research Collaboratory for Structural Bioinformatics, Rutgers University, New Brunswick, NJ†.

Acknowledgements

All NMR data were collected in the laboratory of Angela M. Gronenborn, Laboratory of Chemical Physics, NIDDK, NIH. This research was supported by USDA grant 2003-35302-12930 (PECASE program) and NSF grant IBN-0414073 (to S.M.) and, in part, by the Intramural AIDS Targeted Antiviral Program of the Office of the Director of the National Institute of Health (to A.M.G.). We thank Dr Keyang Ding for help with setting up NMR experiments, and Drs Frank Delaglio and Dan Garrett for software support.

References

1. Hildebrand, J. G. & Shepherd, G. M. (1997). Mechanisms of olfactory discrimination: converging evidence for common principles across phyla. *Annu. Rev. Neurosci.* **20**, 595–631.
2. Buck, L. & Axel, R. (1991). A novel multigene family may encode odorant receptor: A molecular basis for odor recognition. *Cell*, **65**, 175–187.
3. Firestein, S. (2001). How the olfactory system makes sense of scents. *Nature*, **413**, 211–218.
4. Kaissling, K. E. (1996). Peripheral mechanisms of pheromone reception in moths. *Chem. Senses*, **21**, 257–268.
5. Menini, A., Picco, C. & Firestein, S. (1995). Quantal-like current fluctuations induced by odorants in olfactory receptor cells. *Nature*, **373**, 435–437.
6. Pelosi, P. & Maida, R. (1995). Odorant-binding proteins in insects. *Comp. Biochem. Physiol. B*, **111**, 503–514.
7. Roelofs, W. L. (1995). Chemistry of sex attraction. *Proc. Natl Acad. Sci. USA*, **92**, 44–497.
8. Breer, H., Boekhoff, I. & Tareilus, E. (1990). Rapid kinetics of second messenger formation in olfactory transduction. *Nature*, **345**, 65–68.
9. Vogt, R. G. & Riddiford, L. M. (1981). Pheromone binding and inactivation by moth antennae. *Nature*, **293**, 161–163.
10. Steinbrecht, R. A., Ozaki, M. & Ziegelberger, G. (1992). Immunocytochemical localization of pheromone-binding protein in moth antennae. *Cell Tissue Res.* **270**, 287–302.
11. Vogt, R. G., Prestwich, G. D. & Lerner, M. R. (1991). Odorant-binding-protein subfamilies associate with distinct classes of olfactory receptor neurons in insects. *J. Neurobiol.* **22**, 74–84.
12. Tegoni, M., Campanacci, V. & Cambillau, C. (2004). Structural aspects of sexual attraction and chemical communication in insects. *Trends Biochem. Sci.* **29**, 257–264.
13. Maida, R., Ziegelberger, G. & Kaissling, K. E. (2003). Ligand binding to six recombinant pheromone-binding proteins of *Antheraea polyphemus* and *Antheraea pernyi*. *J. Comp. Physiol. B*, **173**, 565–573.
14. Du, G. & Prestwich, G. D. (1995). Protein structure encodes the ligand binding specificity in pheromone binding proteins. *Biochemistry*, **34**, 8726–8732.
15. Maïbèche-Coisné, M., Sobrio, F., Delaunay, T., Lettere, M., Dubroca, J., Jacquin-Joly, E. & Nagnan-Le Meillour, P. (1997). Pheromone binding proteins of the moth *Mamestra brassicae*: specificity of ligand binding. *Insect Biochem. Mol. Biol.* **27**, 213–221.
16. Campanacci, V., Krieger, J., Bette, S., Stargis, J. N., Lartigue, A., Cambillon, H. *et al*. (2001). Revisiting the specificity of *Mamestra brassicae* and *Antheraea polyphemus* pheromone-binding proteins with a fluorescence binding assay. *J. Biol. Chem.* **276**, 20078–20084.
17. Willett, C. S. & Harrison, R. G. (1999). Pheromone binding proteins in the European and Asian corn borers: no protein change associated with pheromone differences. *Insect Biochem. Mol. Biol.* **29**, 277–284.
18. Bette, S., Breer, H. & Krieger, J. (2002). Probing a pheromone binding protein of the silkmoth *Antheraea polyphemus* by endogenous tryptophane fluorescence. *Insect Biochem. Mol. Biol.* **32**, 241–246.
19. Mohl, C., Breer, H. & Krieger, J. (2002). Species-specific pheromonal compounds induce distinct conformational changes of pheromone binding protein subtypes from *Antheraea polyphemus*. *Invert. Neurosci.* **4**, 165–174.
20. Kaissling, K. E. (2001). Olfactory perireceptor and receptor events in moths: a kinetic model. *Chem. Senses*, **26**, 125–150.
21. Pophof, B. (2002). Moth pheromone binding proteins contribute to the excitation of olfactory receptor cells. *Naturwissenschaften*, **89**, 515–518.
22. Sandler, B. H., Nikonova, L., Leal, W. S. & Clardy, J. (2000). Sexual attraction in the silkworm moth: structure of the pheromone-binding-protein-bombykol complex. *Chem. Biol.* **7**, 143–151.
23. Lartigue, A., Gruez, A., Spinelli, S., Riviere, S., Brossut, R., Tegoni, M. & Cambillau, C. (2003). The

† http://www.rscb.org

crystal structure of a cockroach pheromone-binding protein suggests a new ligand binding and release mechanism. *J. Biol. Chem.* **278**, 30213–30218.
24. Lartigue, A., Gruez, A., Briand, L., Blon, F., Bezirard, V., Walsh, M. *et al.* (2004). Sulfur single-wavelength anomalous diffraction crystal structure of a pheromone-binding protein from the honeybee *Apis mellifera* L. *J. Biol. Chem.* **279**, 4459–4464.
25. Kruse, S. W., Zhao, R., Smith, D. P. & Jones, D. N. (2003). Structure of a specific alcohol-binding site defined by the odorant binding protein LUSH from *Drosophila melanogaster*. *Nature Struct. Biol.* **10**, 694–700.
26. Horst, R., Damberger, F., Luginbuhl, P., Guntert, P., Peng, G., Nikonova, L. *et al.* (2001). NMR structure reveals intramolecular regulation mechanism for pheromone binding and release. *Proc. Natl Acad. Sci. USA*, **98**, 14374–14379.
27. Lee, D., Damberger, F. F., Peng, G., Horst, R., Guntert, P., Nikonova, L. *et al.* (2002). NMR structure of the unliganded *Bombyx mori* pheromone-binding protein at physiological pH. *FEBS Letters*, **531**, 314–318.
28. Mohanty, S., Zubkov, S. & Gronenborn, A. M. (2002). The solution NMR structure of Antheraea polyphemus PBP provides new insight into pheromone recognition by pheromone-binding proteins. *J. Mol. Biol.* **337**, 443–451.
29. Wojtasek, H. & Leal, W. S. (1999). Conformational change in the pheromone-binding protein from *Bombyx mori* induced by pH and by interaction with membranes. *J. Biol. Chem.* **274**, 30950–30956.
30. Mohanty, S., Zubkov, S. & Campos-Olivas, R. (2003). ^{1}H, ^{13}C and ^{15}N backbone assignments of the pheromone binding protein from the silk moth *Antheraea* polyphemus (ApolPBP). *J. Biomol. NMR*, **27**, 393–394.
31. McLaughlin, S. (1989). The electrostatic properties of membranes. *Annu. Rev. Biophys. Biophys. Chem.* **18**, 113–136.
32. Kowcun, A., Honson, N. & Plettner, E. (2001). Olfaction in the gypsy moth, Lymantria dispar: effect of pH, ionic strength, and reductants on pheromone transport by pheromone-binding proteins. *J. Biol. Chem.* **276**, 44770–44776.
33. Prestwich, G. D. (1993). Bacterial expression and photoaffinity labeling of a pheromone binding protein. *Protein Sci.* **2**, 420–428.
34. Ferentz, A. & Wagner, G. (2000). NMR spectroscopy: a multifaceted approach to macromolecular structure. *Quart. Rev. Biophys.* **33**, 29–65.
35. Wishart, D. S. & Sykes, B. D. (1994). The ^{13}C chemical-shift index: a simple method for identification of protein secondary structure using ^{13}C chemical-shift data. *J. Biomol. NMR*, **4**, 171–180.
36. Cornilescu, G., Delaglio, F. & Bax, A. (1999). Protein backbone angle restraints from searching a database for chemical shift and sequence homology. *J. Biomol. NMR*, **13**, 289–302.
37. Efimov, A. V. (1984). A novel super-secondary structure of proteins and the relation between the structure and the amino acid sequence. *FEBS Letters*, **166**, 33–38.
38. Chou, K.-C. (2000). Prediction of tight turns and their types in proteins. *Anal. Biochem.* **286**, 1–16.
39. Calderone, V., Berni, R. & Zanotti, G. (2003). High-resolution structures of retinol-binding protein in complex with retinol: pH-induced protein structural changes in the crystal state. *J. Mol. Biol.* **329**, 841–850.
40. MacGillivray, R. T., Bewley, M. C., Smith, C. A., He, Q. Y., Mason, A. B., Woodworth, R. C. & Baker, E. N. (2000). Mutation of the iron ligand His249 to Glu in the N-lobe of human transferring abolishes the dilysine "trigger" but does not significantly affect iron release. *Biochemistry*, **39**, 1211–1216.
41. Langella, E., Improta, R. & Barone, V. (2004). Checking the pH-induced conformational transition of prion protein by molecular dynamics simulations: effect of protonation of histidine residues. *Biophys. J.* **87**, 3623–3632.
42. Henderson, L. M. (1998). Role of histidine identified by mutagenesis in the NADPH oxidase-associated H+ channel. *J. Biol. Chem.* **273**, 3321–3323.
43. Willett, C. S. (2000). Do pheromone binding proteins converge in amino acid sequence when pheromones converge? *J. Mol. Evol.* **50**, 175–183.
44. Renou, M. & Guerrero, A. (2000). Insect parapheromones in olfaction research and semiochemical-based pest control strategies. *Annu. Rev. Entomol.* **45**, 605–630.
45. Trojanowicz, M. (2001). Miniaturized biochemical sensing devices based on planar bilayer lipid membranes. *Fresenius J. Anal. Chem.* **371**, 246–260.
46. Ishida, H., Kobayashi, A., Nakamoto, T. & Moriisumi, T. (1999). Three dimensional odor compass. *IEEE Trans. Robotics Automat.* **15**, 251–257.
47. Delaglio, F., Grzesiek, S., Vuister, G. W., Zhu, G., Pfeifer, J., Bax, A. *et al.* (1995). NMRPipe: a multidimensional spectral processing system based on UNIX pipes. *J. Biomol. NMR*, **6**, 277–293.
48. Johnson, B. A. & Blevins, R. A. (1994). NMRView: a computer program for the visualization and analysis of NMR data. *J. Biomol. NMR*, **4**, 603–614.
49. Mulder, F. A. A., Schipper, D., Bott, R. & Boelens, R. (1999). Altered flexibility in the substrate-binding site of related native and engineered high-alkaline *Bacillus subtilisins*. *J. Mol. Biol.* **292**, 111–123.
50. Güntert, P., Mumenthaler, C. & Wüthrich, K. (1997). Torsion angle dynamics for NMR structure calculation with the new program DYANA. *J. Mol. Biol.* **273**, 283–298.
51. Linger, J. P., Habeck, M., Rieping, W. & Nilges, M. (2003). ARIA: automated NOE assignment and NMR structure calculation. *Bioinformatics*, **19**, 315–316.
52. Koradi, R., Billeter, M. & Wüthrich, K. (1996). MOLMOL: a program for display and analysis of macromolecular structures. *J. Mol. Graph.* **14**, 51–55.
53. Laskowski, R. A., MacArthur, M. W., Moss, D. S. & Thornton, J. M. (1993). PROCHECK - a program to check the stereochemical quality of protein structures. *J. Appl. Crystallog.* **26**, 283–291.
54. Leal, W. S., Chen, A. M. & Erickson, M. L. (2005). Selective and pH-dependent binding of a moth pheromone to a pheromone-binding protein. *J. Chem. Eco.* **31**, 2493–2499.

Edited by M. F. Summers

(Received 28 July 2005; received in revised form 7 October 2005; accepted 7 October 2005)
Available online 27 October 2005